

Desire Backpropagation: A Lightweight Training Algorithm for Multi-Layer Spiking Neural Networks based on Spike-Timing-Dependent Plasticity

Daniel Gerlinghoff^a, Tao Luo^{a,*}, Rick Siow Mong Goh^a, Weng-Fai Wong^b

^a*Institute of High Performance Computing, Agency for Science, Technology and Research (A*STAR), 1 Fusionopolis Way, #16-16 Connexis, Singapore 138632*

^b*Department of Computer Science, National University of Singapore, Computing 1, 13 Computing Drive, Singapore 117417*

Abstract

Spiking neural networks (SNN) are a viable alternative to conventional artificial neural networks when energy efficiency and computational complexity are of importance. A major advantage of SNNs is their binary information transfer through spike trains. The training of SNN has, however, been a challenge, since neuron models are non-differentiable and traditional gradient-based backpropagation algorithms cannot be applied directly. Furthermore, spike-timing-dependent plasticity (STDP), albeit being a spike-based learning rule, updates weights locally and does not optimize for the output error of the network. We present *desire backpropagation*, a method to derive the desired spike activity of neurons from the output error. The loss function can then be evaluated locally for every neuron. Incorporating the desire values into the STDP weight update leads to global error minimization and increasing classification accuracy. At the same time, the neuron dynamics and computational efficiency of STDP are maintained, making it a spike-based supervised learning rule. We trained three-layer networks to classify MNIST and Fashion-MNIST images and reached an accuracy of 98.41% and 87.56%, respectively. Furthermore, we show that desire backpropagation is computationally less complex than backpropagation in traditional neural networks.

Keywords: Spiking Neural Network, Spike-Timing-Dependent Plasticity, Supervised Learning

1. Introduction

Artificial neural networks (ANNs) have been adopted for a wide range of classification tasks, such as image or sound classification. Both training and inference of the model mostly take place on powerful platforms that ideally contain GPUs for acceleration. However, with more neural network applications moving closer to the edge for reasons of data privacy and immediacy, machine learning faces new challenges brought on by the power constraints and limited computing resources found there [1].

Spiking neural networks (SNNs) [2, 3, 4] are a promising technology for deployment of AI at the edge [5]. Experiments, which directly compared them with conventional ANNs, have revealed significant energy and latency advantages [6, 7, 8]. A reason for that is their closer resemblance to biological brains, which inspires new computing paradigms and benefits from custom hardware architectures [9, 10, 11, 12, 13, 14]. SNNs encode information in spike trains, which are series of binary values to indicate the presence (one) or absence (zero) of a spike event. Various methods exist to encode integer or floating point values into spike trains [15, 16, 17, 18, 19]. In this work, we use the firing-rate encoding as detected in the brain by Zhang & Linden [20], where the number of spikes within the fixed-length spike train is proportional to the real value.

*Corresponding author

Email address: 1eto.luo@gmail.com (Tao Luo)

Training the weights of SNNs to yield the correct output spike train, however, poses its own difficulties. Neuron models, such as leaky integrate-and-fire [21], are not differentiable. This means that the classical backpropagation used for ANNs cannot be used directly for SNN training. Instead, there exist three methods for the training of SNNs:

1. *Transfer learning.* An equivalent ANN model is trained using backpropagation while considering the constraints of the SNN. The weights are then transferred onto the SNN [22, 23].
2. *Approximation.* Backpropagation of errors is done using approximations or substitution of the non-differentiable aspects of the neuron model [24, 25, 26, 27].
3. *Direct training methods.* Weights are adjusted based directly on spike events of the neurons. There exist numerous variants of the unsupervised spike-timing-dependent plasticity (STDP) and the supervised Widrow-Hoff learning rule [28, 29, 30, 31].

High classification accuracy has been achieved with the first approach of transfer learning. These algorithms, however, are computationally expensive and may not be suitable for certain use cases, especially on the edge, where the model is required to adapt to changes in the input data through online learning. This work presents a learning algorithm that is based on STDP. It assigns desire values to all neurons, which enables supervision for weight updates to reduce the output error. The learning rule is applied to both output and hidden layers and thus allows the training of multi-layer SNN.

This paper first provides the fundamentals of SNN operation and learning in Section 2. This is followed by a description of our proposed learning rule in Section 3. The results of our experiments are presented in Section 4. An overview over existing spike-based learning algorithms is given in Section 5. Lastly, we draw a conclusion.

2. Background

Like traditional artificial neural networks, SNNs have a layered structure with each layer consisting of an array of neurons. Adjacent neurons are connected via synapses, which can be understood as neuronal junctions to transfer spikes. The two neurons connected by a synapse are referred to as pre-synaptic and post-synaptic neuron, respectively. In this section, we consider a generic fully-connected layer. Post-synaptic neurons of this layer are indexed with o . They receive spikes from pre-synaptic neurons i .

2.1. Neuron model

Neuron models are a mathematical description of the neuron behavior observed in biological experiments. Both the Hodgkin-Huxley model [32] and the Izhikevich model [33] are accurate representations, but are computationally expensive when used for large networks consisting of thousands of neurons. The Spike Response Model (SRM) [34] simulates the neuron's response to a spike using filter kernels. The SRM is a generalization of the Leaky Integrate-and-Fire (LIF) model [21]. Both are biologically plausible, albeit simpler than the first two models. For that reason, they are commonly used for efficient SNN implementations [35, 36, 37]. Our experiments are also based on LIF neurons.

The information transfer between neurons comprises binary spike events, which can occur at any time step $t \in [0, T - 1]$, with T denoting the length of the spike trains. A LIF neuron o retains its internal state, i.e. its membrane potential p_o , between the time steps. Additionally, a leak term $\beta_p \in [0, 1]$ causes a decay of the membrane potential over time. An input spike s_i causes p_o to be increased by weight w_{oi} , where w_{oi} can be a signed value. If the membrane potential surpasses a threshold θ_p , an output spike s_o is fired and the membrane potential is reset. Due to the non-linearity inherent in the neuron model, no additional activation function is needed at the neuron output. The behavior of the LIF neuron can be illustrated as in Figure 1, and expressed by Equation 1.

$$p_o[t + 1] = \beta_p p_o[t] + \sum_i w_{oi} s_i[t] - \theta_p s_o[t] \quad (1)$$

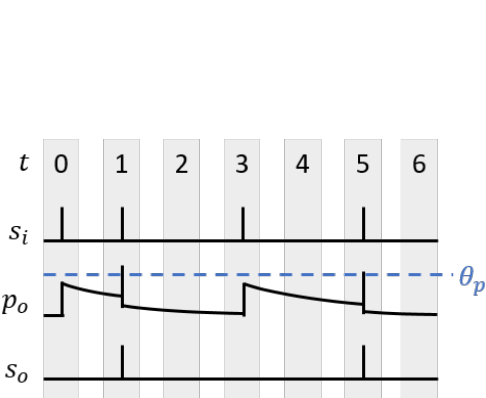


Figure 1: Input spikes s_i and membrane potential p_o of LIF neuron o for every time step $t \in [0, 6]$. If threshold θ_p is exceeded, output spikes s_o are generated.

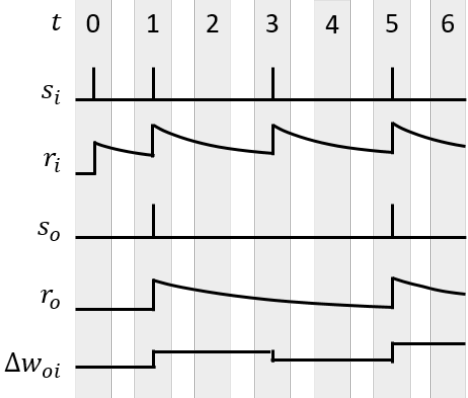


Figure 2: Input spikes s_i and output spikes s_o with respective traces r for six time steps t .

2.2. Spike-timing-dependent plasticity

According to Hebb [38], a weight between two neurons is influenced by the spiking activity of both these neurons. This led to the development of the spike-timing-dependent plasticity (STDP) rule [28, 29], which is a purely spike-based method of training spiking neural networks. It follows the idea of *neurons that fire together wire together* [39, p. 64]. Synaptic weight updates are dependent on relative differences between the spike timing of pre- and post-synaptic neurons. A pre-synaptic spike occurring before a post-synaptic spike is an indication that the pre-synaptic neuron i contributes to the firing of the post-synaptic neuron o . In this case, the connection between i and o is strengthened by increasing weight w_{oi} . And vice versa, if pre-synaptic neuron i fires before post-synaptic neuron o , the weight connecting them is decreased. The update of weight w_{oi} at a time step t can be expressed as:

$$\Delta w_{oi}[t] = \eta^+ s_o[t] r_i[t] - \eta^- s_i[t] r_o[t]. \quad (2)$$

where s_i and s_o are binary spike trains of input and output neuron, respectively. η^+ and η^- are learning rates. Decaying spike traces r_i and r_o account for the time delay between pre- and post-synaptic spikes. The magnitude of the weight update increases as the time period between pre- and post-synaptic spikes becomes shorter. Spike traces are generated by first decaying any existing trace value with an exponential kernel. After that, the trace is incremented in case the neuron fires a spike (see Equation 3). The decay rate $\beta_r < 1$ is a hyper-parameter, which can be trimmed to adjust how the delay between spikes influences the weight update. Figure 2 shows the dynamics of spike traces and weight update expressed by Equation 2.

$$r_{\{o|i\}}[t] = \beta_r * r_{\{o|i\}}[t-1] + s_{\{o|i\}}[t] \quad (3)$$

3. Proposed learning rule

Spike-timing-dependent plasticity is an effective way of adjusting the relationship between neurons in a way that increases their sensitivity to important features present in the dataset [40]. The weight updates are, however, required to be guided, if one wishes to perform supervised learning. In that case, besides extracting features, neuron weights are tuned for reduction of the network's output error. Each neuron in the network is assigned a *desire* value, which is derived from the training labels and determines the direction of the weight update. Through local loss computation, desire values can be assigned to the neurons in the hidden layers.

Since we adopt the backpropagation algorithm, the training routine follows that of traditional deep neural networks. During the forward pass, samples of the training dataset, which are encoded as spike

trains, generate spikes and spike traces in the hidden and output layers. The backward pass employs the desire backpropagation algorithm to derive desire values from training labels and output error. Lastly, the weights are updated following the STDP rule, utilizing spike trains/traces and being guided by desire values.

3.1. Desire-based weight update

The original STDP rule updates the weight w_{oi} whenever there is a spike in either neuron i or neuron o . For supervised learning, however, weight updates should be tied to the activity of the post-synaptic neuron o only, as those are used to compute the subsequent layer and ultimately lead to the output result. Our weight update therefore only takes the post-synaptic spike train s_o and pre-synaptic trace r_i into account. Weights between neurons with higher activity experience larger adjustments, following the idea of Hebbian learning. This is expressed in Equation 4, which applies equally to all weights in the network.

$$\Delta w_{oi}[t] = d_o * \eta s_o[t] r_i[t]. \quad (4)$$

The STDP term of the update equation is not sufficient for supervised learning. That is, instead, accomplished by the desire term d_o , which serves two purposes. Firstly, it decides whether the weight is increased or decreased. Secondly, the weight update is masked if the neuron's spikes have an insignificant influence on the successive layer. Therefore, we define a ternary value $d_o \in \{-1, 0, +1\}$ with the three states describing that:

- $+1$: the neuron o ought to spike and its weights w_{oi} should increase for all i ,
- -1 : the neuron o should not spike and its weights should decrease, or
- 0 : the activity of neuron o is indifferent and the weights should not change

Besides disabling the weight update, a desire of 0 will cause the neuron to not be considered during backpropagation, as will be seen in the next section. The proposed learning rule incorporates STDP, while the desire value depends on the output error. Therefore, it is considered a spike-based supervised learning rule.

3.2. Desire backpropagation

So far, we have used indices i and o to index pre- and post-synaptic neurons of a generic linear layer. In the following, however, there is a differentiation between the output layer and the hidden layers of the network. Figure 3 sketches a network with two subsequent hidden layers G and H , and the last two layers J and K , each with a minimal number of neurons for the sake of readability. We replace indices o and i according to the respective layer descriptors. The figure gives an overview of the steps involved in the computation of the desire values d_k and d_g , based on the output error and local errors, respectively.

3.2.1. Output layer

Supervised learning algorithms aim to reduce the output error of the last network layer. In rate-encoded SNNs, each of the network's output neurons k generates a spike sequence s_k with T binary elements. Accumulation over that sequence yields the spike count. The output error e_k of a neuron is the difference between the normalized spike count and a target \hat{s}_k , given in Equation 5. The target is derived from the training labels. If neuron k represents the target class, it should fire T spikes, and remain silent otherwise.

$$e_k = \frac{1}{T} \sum_{t=0}^{T-1} s_k[t] - \hat{s}_k \quad \text{with} \quad \hat{s}_k = \begin{cases} 1, & \text{if } k \text{ is target class} \\ 0, & \text{otherwise} \end{cases} \quad (5)$$

To quantify the performance of the network we apply the squared error loss function in Equation 6 to the output error e_k . The derivative of the loss function with respect to a single output spike train s_k is required for backpropagation (see Equation 7).

$$L = \frac{1}{2} \sum_k e_k^2 \quad (6)$$

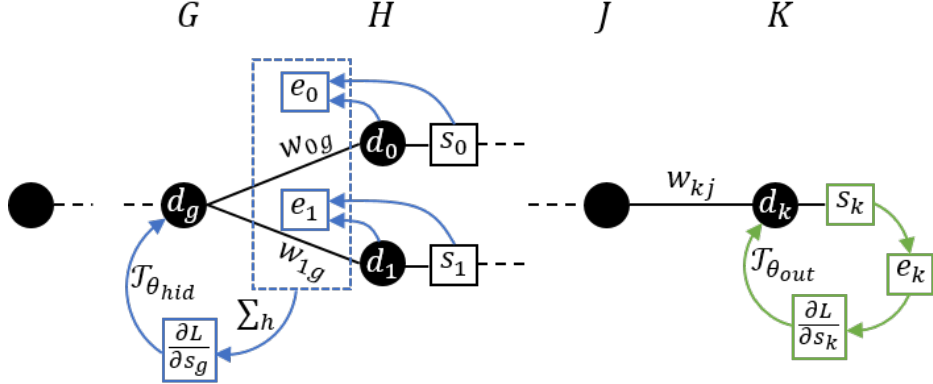


Figure 3: Minimal neural network, which only shows two arbitrary hidden layers G & H and the last two layers J & K . The steps of computing output desire d_k and hidden desire d_g are visualized by the green and blue arrows, respectively.

$$\frac{\partial L}{\partial s_k} = e_k \quad (7)$$

The update of weight w_{kj} is guided by a desire value d_k according to Equation 4. Due to the structural similarity between feed-forward ANN and SNN, we derive the desire by applying gradient decent. The gradient of the loss function with respect to the weight is given in Equation 8, where variables are denoted using the SNN symbols from the previous sections. Due to the non-differential LIF neuron model, we follow [41] and approximate the second term with a straight-through estimator, which has a gradient of one. The first term describes the impact of the weight on the membrane potential p_k . The binary nature of the spikes causes the gradient to be 1, resulting in Equation 9.

$$\frac{\partial L}{\partial w_{kj}} = \frac{\partial p_k}{\partial w_{kj}} \frac{\partial s_k}{\partial p_k} \frac{\partial L}{\partial s_k} \quad (8)$$

$$\frac{\partial L}{\partial w_{kj}} = \frac{\partial L}{\partial s_k} \quad (9)$$

By following the descending gradient of the loss function, we obtain an expression for the desired change in spiking activity, which leads us to our desire value d_k . Since the magnitude of the weight update is determined by the spike timings using STDP, we apply the ternarization function \mathcal{T}_θ (see Equation 10). $\text{sgn}(\cdot)$ is the sign function, which returns -1 for negative and $+1$ for positive values. θ is a threshold value to stabilize the training for small errors, which we call θ_{out} for the output layer in particular. That yields the final expression in Equation 11. In case of the output layer, only weights connecting to the target neuron can get increased, while all others might get decreased.

$$\mathcal{T}_\theta(x) = \begin{cases} \text{sgn } x, & \text{if } |x| > \theta \\ 0, & \text{otherwise} \end{cases} \quad (10)$$

$$d_k = \mathcal{T}_{\theta_{\text{out}}} \left(-\frac{\partial L}{\partial w_{kj}} \right) = \mathcal{T}_{\theta_{\text{out}}} \left(-\frac{\partial L}{\partial s_k} \right) = \begin{cases} -\text{sgn } e_k, & \text{if } |e_k| > \theta_{\text{out}} \\ 0, & \text{otherwise} \end{cases} \quad (11)$$

3.2.2. Hidden layers

Desire backpropagation enables the training of multi-layer neural networks. In contrast to previous methods, such as [42], where the output error of the last layer is backpropagated, we compute the error locally. That allows us to train networks with a higher number of layers. As shown in Figure 3, desire values d_g of hidden layer G are determined based on the desire values and spike trains of layer H .

In the previous section, we derived the dependency of a desire value on the loss gradient with regards to the spike train. To determine this gradient for a hidden neuron, we use the classical backpropagation as a starting point (see Equation 12). Just as before, the straight through estimator and the squared error loss is applied to obtain Equation 13.

$$\frac{\partial L}{\partial s_g} = \sum_h \frac{\partial p_h}{\partial s_g} \frac{\partial s_h}{\partial p_h} \frac{\partial L}{\partial s_h} \quad (12)$$

$$\frac{\partial L}{\partial s_g} = \sum_h w_{hg} * e_h \quad (13)$$

To calculate the loss locally for layer H , the error is only dependent on the spike output and the desire values of this layer. Equation 14 transforms the ternary desire values d_h into targets of $\{0, 1\}$ for the normalized spike count. If the desire value is zero, however, an error cannot be calculated due to the indifference in spiking desire of the neuron. The loss is obtained by squaring the error as done before in Equation 6.

$$e_h = \begin{cases} \frac{1}{T} \sum_{t=0}^{T-1} s_h[t] - (d_h + 1)/2, & \text{if } d_h \neq 0 \\ 0, & \text{otherwise} \end{cases} \quad (14)$$

The desire values of the preceding hidden layer G are obtained by supplying the negative gradient to the ternarization function \mathcal{T}_θ with a threshold θ_{hid} specific for hidden layers. The final expression of a desire value d_g is given in Equation 15. In summary, the computation only relies on desire values, spike trains and weights of layer H .

$$d_g = \mathcal{T}_{\theta_{\text{hid}}} \left(-\frac{\partial L}{\partial s_g} \right) = \begin{cases} -\text{sgn}(\sum_h w_{hg} e_h), & \text{if } |\sum_h w_{hg} e_h| > \theta_{\text{hid}} \\ 0, & \text{otherwise} \end{cases} \quad (15)$$

Using Equation 15, the desire values of layer G are set such that the desire in layer H is satisfied. Although a pre-synaptic neuron g cannot fulfill the desire of all post-synaptic neurons d_h , the sum over all $w_{hg} e_h$ gives an indication about the preference in the spiking activity of g . If neuron g does not significantly contribute to the average fulfillment of the desire in layer H , no adjustment is made to its weights. This is reflected by a desire d_g of zero.

If the network has been trained and has reached an equilibrium, the local errors are small enough to draw desire values to zero. In that case, weights theoretically stabilize and are not adjusted. The network's ability to generalize depends, however, on the number of neurons and layers. In practise, the output error will not be zero for all samples, which leads to continuing weight adjustments even towards the end of the training.

3.3. Dropout

After many training epochs, the accuracy of classifying the training dataset usually increases, while the accuracy on the validation dataset might remain unchanged or even decrease. This is the phenomenon of overfitting. Dropout [43] is a technique to increase the generality of a network model, and has been shown to be effective for SNNs [44].

Dropout simulates the training of multiple neural networks by randomly excluding neurons of each layer during the training phase. During the evaluation phase, dropout is not applied, which is equivalent to combining the results of all those neural networks. The parameter P_{drop} gives the probability of a neuron to be dropped out. Since the neuron configuration needs to remain constant for all time steps, a binary dropout mask m is generated for each layer at the beginning of each sample. An input neuron i , which is silenced by $m_i = 0$, does not contribute to the desire backpropagation and does not get its weights updated.

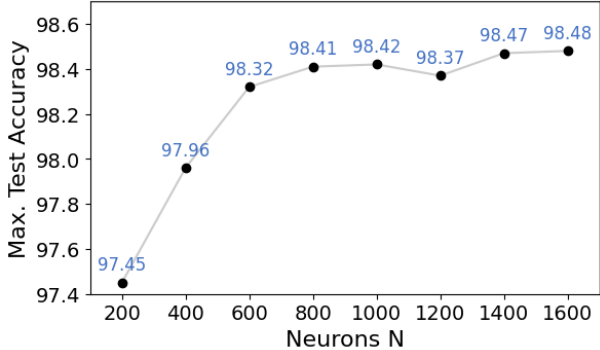


Figure 4: Classification accuracy (in %) plotted against the number of hidden neurons N in a 3-layer MLP architected as $784 - 2N - N - 10$ and $L = 20$.

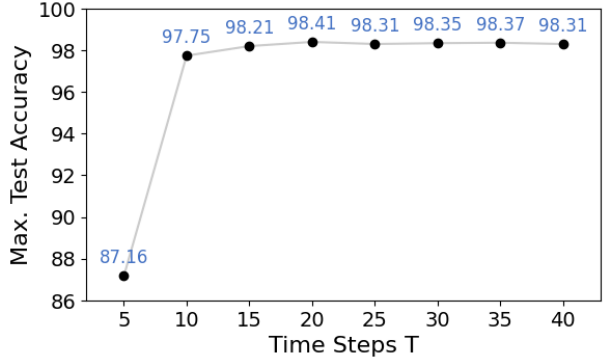


Figure 5: Accuracy (in %) versus spike train length / number of time steps T with N set to 800.

Dropout leads to a reduction of the number of spikes arriving at the next layer. To compensate for that, the influence of the active neurons on the membrane potential is increased by a factor $1/(1 - P_{\text{drop}})$. Equation 1 for the training phase is modified to include dropout as follows:

$$p_o[t+1] = \beta_p p_o[t] + w_{oi} s_i[t] * \frac{m_i}{1 - P_{\text{drop}}} - s_o[t]. \quad (16)$$

4. Experiments and results

4.1. Spike generation

For the sake of comparability, we used popular image datasets for classification. Since those datasets are only available as two-dimensional pixel data, spike trains with additional timing information need to be generated. For rate encoding, the number of spikes in the input spike train is proportional to the brightness value of the respective pixel. We do not carry out any data preprocessing or augmentation.

Our input layer contains LIF neurons (see Section 2.1), which increment their membrane potential at each time step by a constant, which is equal to the the brightness value of the input $\in [0, 1]$. The membrane potential is not decayed, i.e. $\beta_p = 1$. A brighter pixel leads to larger increments of the membrane potential p_o at every time step. Hence, the threshold θ_p is reached faster and more often and more spikes are generated. The dropout rate P_{drop} can be adjusted separately for the input layer.

4.2. MNIST classification

We trained a multilayer perceptron (MLP) on 60,000 training images of the handwritten digits dataset MNIST [45]. The accuracy values in this section were obtained from the 10,000 test images. The network consists of three fully-connected layers with a variable neuron count of $784 - 2N - N - 10$. We use a variable number of time steps T for the spike trains. Our PyTorch implementation of the spiking neural network allows an exponential decay of the learning rate. We start off with a learning rate $\eta = 1 * 10^{-5}$, which is reduced by 4% at the end of every training epoch. Training is carried out for a total of 150 epochs. Other hyper-parameters include the firing threshold $\theta_p = 1.0$, the desire thresholds $\theta_{\text{hid}} = 0.05$ and $\theta_{\text{out}} = 0.30$, and the dropout rate $P_{\text{drop}} = 30\%$ for hidden layers and no dropout at the input layer.

A classification is deemed correct, if the output neuron, which corresponds to the target class, fires the strict maximum number of spikes. That is, all other output neurons fire fewer spikes. We plotted the test accuracy against the number of neurons N and time steps T as seen in Figures 4 and 5, respectively. A higher number of neurons increases the ability of the network to recognize details in the input samples. As expected, the classification accuracy of our network tends to increase with the neuron count. Saturation occurs when additional neurons do not lead to a considerable increase in accuracy. The most efficient network

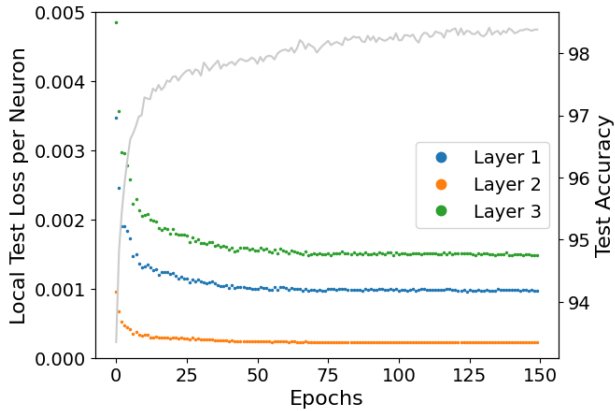


Figure 6: Average local test losses for each neuron in layer 1, 2 and 3 throughout the training with 150 epochs. Accuracy on test dataset for each epoch (gray line).

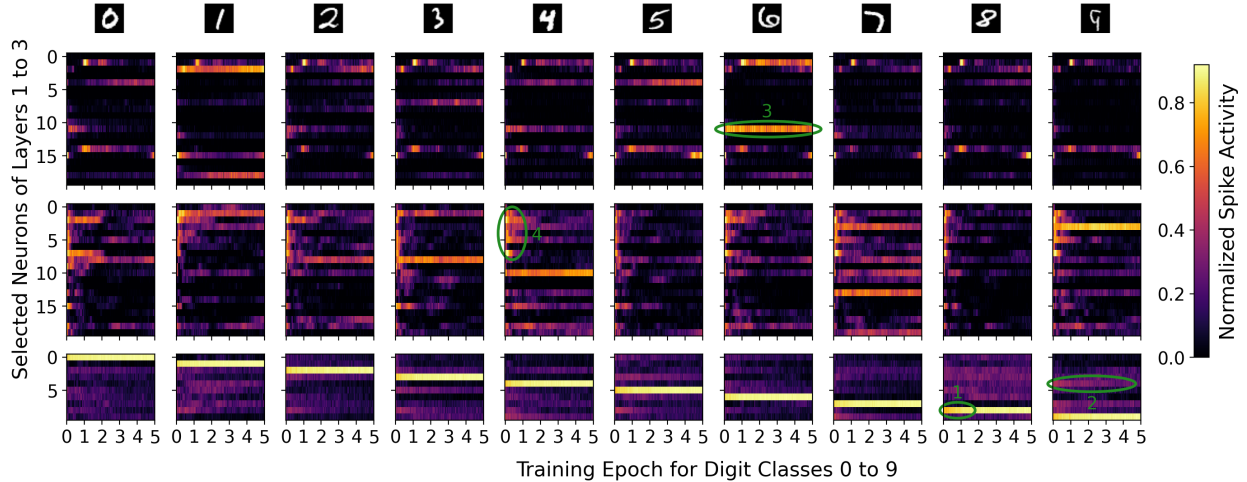


Figure 7: Color-coded spike activity of neurons in the three layers over five training epochs. Plots are separated into columns for each of the ten handwritten digits 0 to 9. Four regions of interest are marked by green circles.

structure contains $2 * 800 + 800 = 2400$ hidden neurons, with $N = 800$. It reaches a test accuracy of 98.41%. The highest accuracy of 98.48% can be reached at the cost of increase in neurons. With regards to Figure 5, the hyperparameter tuning was performed for $T = 20$, explaining the peak accuracy for this configuration. With spike-based learning, every time step influences the update of weights. Although longer spike trains can represent more information, it also requires additional adjustments of learning rate and thresholds. Using only five time steps causes significant information loss in the activations, which is reflected in the drop of classification accuracy.

For a training with parameters $N = 800$ and $T = 20$, we analyze the learning rule's impact on the neurons of the network. After each epoch, we evaluate the network with the test dataset and record the local loss of each neuron in the three layers according to Equation 6. The result is plotted in Figure 6, which shows a clear decrease in local losses throughout the training process. Concurrently, the classification accuracy tends to increase. A deeper insight in the spiking activity of individual neurons for the first five training epochs is given in Figure 7, with special regions of interest marked by green circles. We randomly selected 20 neurons from the two hidden layers and, together with the ten output neurons, plot their color-coded relative spike count. The activity is measured separately for each of the ten classes of digits 0 to 9. The last row of plots

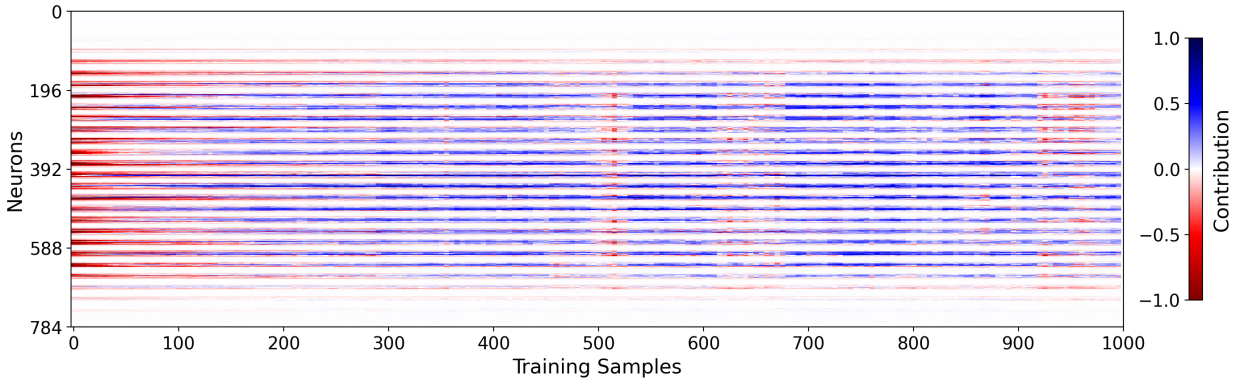


Figure 8: Contribution of each of the input layer neurons to satisfy on average the desire of the neurons in the next layer, measured for the first 1000 samples in the first training epoch. White color represents no contribution, while the shades of red and blue stand for negative and positive contribution, respectively.

represents the output layer and, as expected, the spike activity is concentrated at the correct output neuron for each class, i.e. neuron 0 spikes for class 0, etc. One can observe that the activity of target neurons is initially lower and increases throughout the training (region 1). Accordingly, non-target output neurons tends transition towards lower activity (region 2). In the hidden layers, represented by the upper two rows of plots, neurons are shown to be sensitive to certain input classes. For example, neuron 11 in the first layer spikes for class 6, but not for any other class (region 3). This sensitivity is established mainly within the first training epoch. Bright regions at the left edges of some plots show that, initially, many neurons were active and later silenced as result of the training (region 4). Lastly, in Figure 8, colors encode how a neuron contributes on average to satisfy the desire of the neurons in the next layer. Contribution is a function of layer weights, input/output spikes, and desire values. Thereby, red represents a bad influence, meaning that spike activity in this neuron will cause neurons in the next layer to fire in an undesired manner. Blue color reflects positive contribution to the overall desire satisfaction. The contribution was measured for each of the 784 neurons of the first layer over the first 1000 training samples of the first epoch. Because neurons at the edges of the input image remain silent for all samples, their contribution is zero throughout. The others display negative contribution at the start of the training, gradually improving as the network is exposed to more training samples. The red patch at around 500 samples indicate a temporary drop in contribution, likely caused by out-of-distribution training samples.

Table 1 compares our desire backpropagation with state-of-the-art works for SNN training. For a fair comparison, we include learning rules, which perform supervised spike-timing-driven weight updates, and employ fully-connected layers. Our method outperforms most of those learning algorithms in terms of accuracy, such as [46, 47, 48, 42, 41, 49, 50, 51, 52, 53]. Those achieving a higher accuracy [54, 55] require a significant increase in the number of neurons and/or time steps. CNN architectures [48, 55] especially require considerably more computational effort, with only a small impact on accuracy. While [47, 41, 53] show advantages in terms of neuron count, they require feedback weights in addition to the feed-forward weights, which might not be suitable for memory-constraint devices. While all listed learning rules are able to train at least the last network layer in a supervised, some learning rules cannot be generalized for deeper networks [42, 55, 49]. The table shows that desire backpropagation is a competitive learning rule, which achieves high accuracy while keeping the number of neurons low.

4.3. Fashion-MNIST classification

Just like MNIST, Fashion-MNIST [56] consists of 60,000 training and 10,000 validation images that are 28x28 pixels. They belong to ten kinds of clothing, such as shirts, trousers, and shoes. The photographic nature of the images contains more detail than digits of the MNIST dataset and are hence more challenging to classify correctly. However, for the same reason, Fashion-MNIST is considered a more realistic dataset

Table 1: Comparison of state-of-the-art learning rules for the MNIST dataset with regards to accuracy (in %), number of neurons and time steps.

Model	Layers	Learning Rule	Acc.	Neurons	T.steps
Shrestha (2017) [46]	2 FC	Stable STDP	89.7	1600	200
Neftci (2017) [47]	3 FC	eRBP	98.0	1000	125
Kheradpisheh (2018) [48]	CNN	STDP+SVM	98.4	12220	30
Zhang (2018) [54]	2 FC	Equ. Learn.+STDP	98.5	4500	100
Tavanaei (2019) [42]	3 FC	BP-STDP	97.2	650	10
Falez (2019) [55]	CNN	STDP+SVM	98.6	35328	—
Shrestha (2019) [41]	3 FC	EMSTDP	97.3	1000	200
Hao (2020) [49]	2 FC	DA-STDP	96.7	10000	700
Comsa (2020) [50]	2 FC	Error BP	98.0	340	10
Mirsadeghi (2021) [52]	2 FC	STiDi-BP	97.4	500	300
Liu (2021) [51]	2 FC	SSTDP	98.1	300	16
Tang (2021) [53]	3 FC	BioGrad	98.1	600	20
This work	3 FC	STDP+Desire BP	98.4	2400	20

for computer vision applications [49]. We train a network with three fully-connected layers and 784 – 1000 – 100 – 10 neurons. Spike trains have a length of $T = 20$. A total of 600 epochs had to be computed due to higher dropout rates of 40% and 5% for hidden and input layers, respectively. All other hyperparameters are equal to the ones used for MNIST classification in Section 4.2.

With those settings, we achieved a classification accuracy of 87.56%. The comparison with Shrestha et al. [41] and Hao et al. [49] reflects the result of the MNIST classification (see Table 2). Desire backpropagation achieved the highest accuracy, while using either a similar number of neurons or less.

Table 2: Results and comparison of Fashion-MNIST classification with indication of accuracy (in %), number of neurons and time steps.

Model	Layers	Learning Rule	Acc.	Neurons	T.steps
Shrestha (2019) [41]	3 FC	EMSTDP	86.1	1000	200
Hao (2020) [49]	2 FC	DA-STDP	85.3	6400	—
This work	3 FC	STDP+Desire BP	87.6	1100	20

4.4. Computational complexity

Spiking neural networks have been touted as an efficient alternative to conventional artificial neural networks. In this section, we take a deeper look into the computational complexity of desire backpropagation. For forward pass, backward pass and weight update of a single neuron, the number of operations is determined and compared with classical backpropagation in Table 3. It shows the dependency of the SNN forward pass on the number of time steps T and the number of inputs I . Binary spikes allow the use of conditional statements instead of multiplications. Only one multiplication is needed for the decay of the membrane potential, whereas ANNs require multiplications and additions for all I inputs. In the backward pass, Desire BP replaces one multiplication with an addition due to the local computation of losses. One conditional statement is used in the ternarization function. The ternary nature of the desire values benefits the weight update, as one multiplication operation can be saved. Multiplications are computationally more

Table 3: Comparison of operations needed for three sub-processes using desire backpropagation and classical backpropagation. I/O are the numbers of inputs/outputs to a neuron, T is the number of time steps.

Process	SNN: Desire BP			ANN: BP	
	Mult.	Add.	Cond.	Mult.	Add.
Forward	1	TI	TI	I	I
Backward	O	$2O$	1	$2O$	O
Update	1	–	1	2	–

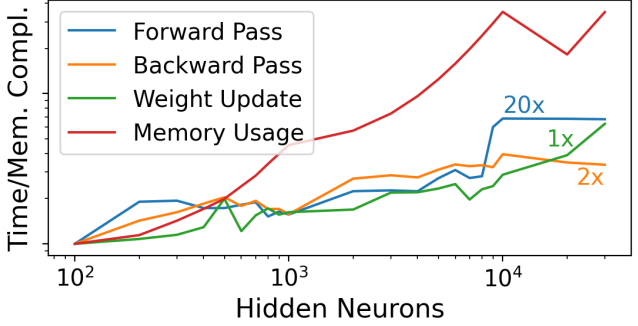


Figure 9: Normalized execution time of forward pass, backward pass, and weight update, and memory usage during training. Numbers on plot lines are the scaling factors to indicate relationship between execution times.

expensive than additions, which are in turn more expensive than conditional statements. Spike-based processing in combination with our learning rule can therefore be expected to be more computationally efficient overall.

From table 3 we can derive linear time complexity with respect to inputs I and outputs O . To confirm this hypothesis, an SNN for the classification of MNIST digits was constructed, consisting of input, hidden, and output layer. The number of neurons in the hidden layer is varied in logarithmic steps from 100 to 30000. We then executed the training on an NVIDIA GeForce RTX 2080 Ti GPU and measured the execution time of forward pass, backward pass and weight update. In addition, we recorded the memory utilization of the process running the Python script.

Before displaying the results in Figure 9, the data were individually normalized in terms of offset and range, allowing a direct comparison of the dependency on the hidden neuron number. The plot uses logarithmic scale for both horizontal and vertical axes. As expected, a roughly linear trend can be detected for time complexity. Because each neuron in the network comprises an equal number of internal variables, the memory shows linear behaviour as well. Due to parallel execution within the GPU, execution time does not always increase with larger neuron count. Instead, it maintains a constant level before increasing by a bigger step. The absolute relationship between the execution time for different processes is indicated by the scaling factors on the plot lines. The forward pass takes around 20 \times more time to run. With the number of time steps being 20, the forward pass has to execute 20 times, while backward pass and weight update is only performed once.

5. Related research

The learning rules of spiking neural networks are inspired by the inner workings of biological brains. In order for a neuron model and learning rule to be deemed biologically plausible, training and inference should be spike-based, i.e., operate on the temporal information of the spike train and interface using spike information [49]. Spike-timing-dependent plasticity is such a rule, that only relies on locally available spike information, and was used for unsupervised learning [57]. The same team of researchers enhanced this method by learning neurons in competition through a winner-takes-all mechanism that inhibits the spiking of laterally adjacent neurons to prevent them from learning the same patterns [58]. Kheradpisheh et al. [48] coupled STDP-based network layers with a linear SVM classifier to enable supervised learning. Similarly, Thiele et al. [59] uses a custom event-based classifier to allow the learning to depend on the output error.

To use the STDP rule directly for supervised learning, it was separated into the STDP and anti-STDP processes, which refer to weight strengthening and weakening, respectively [30, 60, 61]. In his doctoral dissertation, Ponulak [30] showed how to train a network for a timing-accurate spike sequence. The STDP process is applied whenever a spike in the desired sequence occurs, while anti-STDP is applied for every

actual output spike. Once the actual spike train matches the desired one, STDP and anti-STDP process counteract each other and weights are not modified. A *learning window* is used for the spike timing to scale the magnitude of the weight update. Ponulak’s learning rule was adopted by Wang et al. [61]. Weights of their output layer are updated at the time of actual output spikes only. The sign of the weight update is determined by whether or not the output neuron is desired to spike. The idea of spiking desire was used earlier by the Tempotron [62] to determine the sign of the weight update, while the magnitude is proportional to the output error. In a similar manner, PBSNLR [63] tries to match the output spike timings with a desired spike train by adjusting weights, whenever there is a spike at an undesired time or a failure to spike at a desired time step. Those rules are only applied to a single-layer MLP or the output layer of the SNN as hidden neurons lack the information about spiking desire.

Other spike-based supervised learning algorithms are based on the Widrow-Hoff rule [31, 64]. It adjusts the neurons of the output layer according to the contribution to their respective output errors. This rule is, again, applied to the last layer due to the ability to directly compute the output error. Tavanaei & Maida [42] improved this rule to train the last two layers of a network.

Seeing the benefits of spike-based learning, recent works have adopted traditional backpropagation to SNN neuron models. Shrestha et al. [41] uses error neurons to record local errors during the forward pass. They exhibit the same neuron behaviour as forward neurons. Mirsadeghi et al. [52] approximate error backpropagation in SNN and execute the weight adjustment based on STDP principles. Liu et al. [51] approximate partial derivatives of the backpropagation with an STDP-like expression, enabling the error to be propagated back through the network.

Learning of spiking neural networks has also been adopted from conventional artificial neural networks. However, learning rules do often not adhere to the characteristic of biological plausibility mentioned earlier. Wu et al. [65] apply error backpropagation to SNNs by updating the synaptic weights based on the total number of output spikes rather than spike timing. Similarly, GLSNN [66] does not consider the temporal relation between spikes when updating their weight through feedback alignment.

6. Conclusion

In this paper, we propose desire backpropagation, a novel lightweight learning algorithm for spiking neural networks. With STDP as its foundation, our learning rule utilizes the benefits of spike-based learning such as energy efficiency and biological plausibility. To enable multi-layer learning, we introduced the ternary spiking desire of a neuron. It determines, whether the weight needs to be increased or decreased during the STDP update to minimize the output error. The desire value of the output layer can directly be derived from the labels of the training samples. For hidden layers, we utilized local losses, which can be calculated based on already propagated desire values. The backpropagation sets desire values in a way that helps satisfying the desire of the successive layer. The ternary desire values are coupled with a binary dropout mask to avoid overfitting of the model.

We tested our learning rule on the MNIST and Fashion-MNIST datasets and achieved remarkable classification accuracy of 98.41% and 87.56%, respectively. It not only shows superior accuracy compared to many other learning rules, but also uses less neurons and time steps than most other algorithms. We further compared the required operations with classical backpropagation and demonstrated its advantages in terms of computational complexity. Its performance and efficiency makes desire backpropagation a potential candidate for deployment and online learning on edge devices.

7. Acknowledgement

This work was supported by the Singapore Government’s Research, Innovation and Enterprise 2020 Plan (Advanced Manufacturing and Engineering domain) under Grant A1687b0033.

References

- [1] W. Li, M. Liewig, A survey of ai accelerators for edge environment, in: World Conference on Information Systems and Technologies, Springer, 2020, pp. 35–44.
- [2] D. Neil, M. Pfeiffer, S.-C. Liu, Learning to be efficient: Algorithms for training low-latency, low-compute deep spiking neural networks, in: Proceedings of the 31st annual ACM symposium on applied computing, 2016, pp. 293–298.
- [3] C. Farabet, R. Paz, J. Pérez-Carrasco, C. Zamarreño, A. Linares-Barranco, Y. LeCun, E. Culurciello, T. Serrano-Gotarredona, B. Linares-Barranco, Comparison between frame-constrained fix-pixel-value and frame-free spiking-dynamic-pixel convnets for visual processing, *Frontiers in neuroscience* 6 (2012) 32.
- [4] P. O'Connor, D. Neil, S.-C. Liu, T. Delbrück, M. Pfeiffer, Real-time classification and sensor fusion with a spiking deep belief network, *Frontiers in neuroscience* 7 (2013) 178.
- [5] H. Lu, J. Liu, Y. Luo, Y. Hua, S. Qiu, Y. Huang, An autonomous learning mobile robot using biological reward modulate stdp, *Neurocomputing* 458 (2021) 308–318.
- [6] H. Lee, C. Kim, S. Lee, E. Baek, J. Kim, An accurate and fair evaluation methodology for snn-based inferencing with full-stack hardware design space explorations, *Neurocomputing* 455 (2021) 125–138.
- [7] P. Blouw, X. Choo, E. Hunsberger, C. Eliasmith, Benchmarking keyword spotting efficiency on neuromorphic hardware, in: Proceedings of the 7th Annual Neuro-inspired Computational Elements Workshop, 2019, pp. 1–8.
- [8] E. Stamatias, D. Neil, F. Galluppi, M. Pfeiffer, S.-C. Liu, S. Furber, Scalable energy-efficient, low-latency implementations of trained spiking deep belief networks on spinnaker, in: 2015 International Joint Conference on Neural Networks (IJCNN), IEEE, 2015, pp. 1–8.
- [9] L. Yang, H. Zhang, T. Luo, C. Qu, M. T. L. Aung, Y. Cui, J. Zhou, M. M. Wong, J. Pu, A. T. Do, et al., Coreset: Hierarchical neuromorphic computing supporting large-scale neural networks with improved resource efficiency, *Neurocomputing* 474 (2022) 128–140.
- [10] T. Luo, L. Yang, H. Zhang, C. Qu, X. Wang, Y. Cui, W.-F. Wong, R. S. M. Goh, Nc-net: Efficient neuromorphic computing using aggregated sub-nets on a crossbar-based architecture with non-volatile memory, *IEEE Transactions on Computer-Aided Design of Integrated Circuits and Systems*.
- [11] M. T. L. Aung, C. Qu, L. Yang, T. Luo, R. S. M. Goh, W.-F. Wong, Deepfire: Acceleration of convolutional spiking neural network on modern field programmable gate arrays, in: 2021 31st International Conference on Field-Programmable Logic and Applications (FPL), IEEE, 2021, pp. 28–32.
- [12] D. Gerlinghoff, Z. Wang, X. Gu, R. S. M. Goh, T. Luo, E3ne: An end-to-end framework for accelerating spiking neural networks with emerging neural encoding on fpgas, *IEEE Transactions on Parallel and Distributed Systems*.
- [13] J. Lin, J.-S. Yuan, A scalable and reconfigurable in-memory architecture for ternary deep spiking neural network with reram based neurons, *Neurocomputing* 375 (2020) 102–112.
- [14] G. Zhang, B. Li, J. Wu, R. Wang, Y. Lan, L. Sun, S. Lei, H. Li, Y. Chen, A low-cost and high-speed hardware implementation of spiking neural network, *Neurocomputing* 382 (2020) 106–115.
- [15] R. Kempter, W. Gerstner, J. L. Van Hemmen, Spike-based compared to rate-based hebbian learning, *Advances in neural information processing systems* 11 (1999) 125–131.
- [16] A. Borst, F. E. Theunissen, Information theory and neural coding, *Nature neuroscience* 2 (11) (1999) 947–957.
- [17] R. Gütig, To spike, or when to spike?, *Current opinion in neurobiology* 25 (2014) 134–139.
- [18] H. Tang, D. Cho, D. Lew, T. Kim, J. Park, Rank order coding based spiking convolutional neural network architecture with energy-efficient membrane voltage updates, *Neurocomputing* 407 (2020) 300–312.
- [19] A. Sboev, A. Serenko, R. Rybka, D. Vlasov, Solving a classification task by spiking neural network with stdp based on rate and temporal input encoding, *Mathematical Methods in the Applied Sciences* 43 (13) (2020) 7802–7814.
- [20] W. Zhang, D. J. Linden, The other side of the engram: experience-driven changes in neuronal intrinsic excitability, *Nature Reviews Neuroscience* 4 (11) (2003) 885–900.
- [21] C. Koch, I. Segev, Methods in neuronal modeling: From ions to networks, MIT press, 1998.
- [22] B. Rueckauer, I.-A. Lungu, Y. Hu, M. Pfeiffer, S.-C. Liu, Conversion of continuous-valued deep networks to efficient event-driven networks for image classification, *Frontiers in neuroscience* 11 (2017) 682.
- [23] A. Sengupta, Y. Ye, R. Wang, C. Liu, K. Roy, Going deeper in spiking neural networks: Vgg and residual architectures, *Frontiers in neuroscience* 13 (2019) 95.
- [24] S. M. Bohte, J. N. Kok, J. A. La Poutré, Spikeprop: Backpropagation for networks of spiking neurons, in: ESANN, 2000, pp. 419–424.
- [25] J. C. Thiele, O. Bichler, A. Dupret, Spikegrad: An ann-equivalent computation model for implementing backpropagation with spikes, *arXiv preprint arXiv:1906.00851*.
- [26] S. B. Shrestha, G. Orchard, Slayer: Spike layer error reassignment in time, *Advances in Neural Information Processing Systems 2018-Decem* (2018) 1412–1421.
- [27] G. Qiao, N. Ning, Y. Zuo, S. Hu, Q. Yu, Y. Liu, Direct training of hardware-friendly weight binarized spiking neural network with surrogate gradient learning towards spatio-temporal event-based dynamic data recognition, *Neurocomputing* 457 (2021) 203–213.
- [28] W. Gerstner, R. Kempter, J. L. Van Hemmen, H. Wagner, A neuronal learning rule for sub-millisecond temporal coding, *Nature* 383 (6595) (1996) 76–78.
- [29] N. Caporale, Y. Dan, Spike timing-dependent plasticity: A hebbian learning rule, *Annu. Rev. Neurosci.* 31 (2008) 25–46.
- [30] F. Ponulak, Supervised learning in spiking neural networks with resume method, *Phd*, Poznan University of Technology 46 (2006) 47.

[31] A. Mohammed, S. Schliebs, S. Matsuda, N. Kasabov, Span: Spike pattern association neuron for learning spatio-temporal spike patterns, *International journal of neural systems* 22 (04) (2012) 1250012.

[32] A. L. Hodgkin, A. F. Huxley, A quantitative description of membrane current and its application to conduction and excitation in nerve, *The Journal of physiology* 117 (4) (1952) 500–544.

[33] E. M. Izhikevich, Simple model of spiking neurons, *IEEE Transactions on neural networks* 14 (6) (2003) 1569–1572.

[34] W. Gerstner, R. Ritz, J. L. Van Hemmen, Why spikes? hebbian learning and retrieval of time-resolved excitation patterns, *Biological cybernetics* 69 (5) (1993) 503–515.

[35] H. Fang, Z. Mei, A. Shrestha, Z. Zhao, Y. Li, Q. Qiu, Encoding, model, and architecture: systematic optimization for spiking neural network in fpgas, in: 2020 IEEE/ACM International Conference On Computer Aided Design (ICCAD), IEEE, 2020, pp. 1–9.

[36] A. S. Cassidy, P. Merolla, J. V. Arthur, S. K. Esser, B. Jackson, R. Alvarez-Icaza, P. Datta, J. Sawada, T. M. Wong, V. Feldman, et al., Cognitive computing building block: A versatile and efficient digital neuron model for neurosynaptic cores, in: The 2013 International Joint Conference on Neural Networks (IJCNN), IEEE, 2013, pp. 1–10.

[37] B. Girau, C. Torres-Huitzil, Massively distributed digital implementation of an integrate-and-fire legion network for visual scene segmentation, *Neurocomputing* 70 (7-9) (2007) 1186–1197.

[38] D. O. Hebb, The organization of behavior; a neuropsychological theory, *A Wiley Book in Clinical Psychology* 62 (1949) 78.

[39] C. J. Shatz, The developing brain, *Scientific American* 267 (3) (1992) 60–67.

[40] Q. Fu, H. Dong, An ensemble unsupervised spiking neural network for objective recognition, *Neurocomputing* 419 (2021) 47–58.

[41] A. Shrestha, H. Fang, Q. Wu, Q. Qiu, Approximating back-propagation for a biologically plausible local learning rule in spiking neural networks, in: *Proceedings of the International Conference on Neuromorphic Systems*, 2019, pp. 1–8.

[42] A. Tavanaei, A. Maida, Bp-stdp: Approximating backpropagation using spike timing dependent plasticity, *Neurocomputing* 330 (2019) 39–47.

[43] N. Srivastava, G. Hinton, A. Krizhevsky, I. Sutskever, R. Salakhutdinov, Dropout: a simple way to prevent neural networks from overfitting, *The journal of machine learning research* 15 (1) (2014) 1929–1958.

[44] C. Lee, S. S. Sarwar, P. Panda, G. Srinivasan, K. Roy, Enabling spike-based backpropagation for training deep neural network architectures, *Frontiers in neuroscience* 14.

[45] Y. LeCun, The mnist database of handwritten digits, <http://yann. lecun. com/exdb/mnist/>.

[46] A. Shrestha, K. Ahmed, Y. Wang, Q. Qiu, Stable spike-timing dependent plasticity rule for multilayer unsupervised and supervised learning, in: *2017 international joint conference on neural networks (IJCNN)*, IEEE, 2017, pp. 1999–2006.

[47] E. O. Neftci, C. Augustine, S. Paul, G. Detorakis, Event-driven random back-propagation: Enabling neuromorphic deep learning machines, *Frontiers in neuroscience* 11 (2017) 324.

[48] S. R. Kheradpisheh, M. Ganjtabesh, S. J. Thorpe, T. Masquelier, Stdp-based spiking deep convolutional neural networks for object recognition, *Neural Networks* 99 (2018) 56–67.

[49] Y. Hao, X. Huang, M. Dong, B. Xu, A biologically plausible supervised learning method for spiking neural networks using the symmetric stdp rule, *Neural Networks* 121 (2020) 387–395.

[50] I. M. Comsa, K. Potempa, L. Versari, T. Fischbacher, A. Gesmundo, J. Alakuijala, Temporal coding in spiking neural networks with alpha synaptic function, in: *ICASSP 2020-2020 IEEE International Conference on Acoustics, Speech and Signal Processing (ICASSP)*, IEEE, 2020, pp. 8529–8533.

[51] F. Liu, W. Zhao, Y. Chen, Z. Wang, T. Yang, L. Jiang, Sstdp: Supervised spike timing dependent plasticity for efficient spiking neural network training, *Frontiers in Neuroscience* 15.

[52] M. Mirsadeghi, M. Shalchian, S. R. Kheradpisheh, T. Masquelier, Stidi-bp: Spike time displacement based error back-propagation in multilayer spiking neural networks, *Neurocomputing* 427 (2021) 131–140.

[53] G. Tang, N. Kumar, I. Polykretis, K. P. Michmizos, Biograd: Biologically plausible gradient-based learning for spiking neural networks, *arXiv preprint arXiv:2110.14092*.

[54] T. Zhang, Y. Zeng, D. Zhao, M. Shi, A plasticity-centric approach to train the non-differential spiking neural networks, in: *Proceedings of the AAAI Conference on Artificial Intelligence*, Vol. 32, 2018, pp. 620–627.

[55] P. Falez, P. Tirilly, I. M. Bilasco, P. Devienne, P. Boulet, Multi-layered spiking neural network with target timestamp threshold adaptation and stdp, in: *2019 International Joint Conference on Neural Networks (IJCNN)*, IEEE, 2019, pp. 1–8.

[56] H. Xiao, K. Rasul, R. Vollgraf, Fashion-mnist: a novel image dataset for benchmarking machine learning algorithms, *arXiv preprint arXiv:1708.07747*.

[57] T. Masquelier, S. J. Thorpe, Unsupervised learning of visual features through spike timing dependent plasticity, *PLoS Comput Biol* 3 (2) (2007) e31.

[58] T. Masquelier, S. J. Thorpe, Learning to recognize objects using waves of spikes and spike timing-dependent plasticity, in: *The 2010 International Joint Conference on Neural Networks (IJCNN)*, IEEE, 2010, pp. 1–8.

[59] J. C. Thiele, O. Bichler, A. Dupret, A timescale invariant stdp-based spiking deep network for unsupervised online feature extraction from event-based sensor data, in: *2018 International Joint Conference on Neural Networks (IJCNN)*, IEEE, 2018, pp. 1–8.

[60] I. Sporea, A. Grüning, Supervised learning in multilayer spiking neural networks, *Neural computation* 25 (2) (2013) 473–509.

[61] J. Wang, A. Belatreche, L. Maguire, T. M. McGinnity, An online supervised learning method for spiking neural networks with adaptive structure, *Neurocomputing* 144 (2014) 526–536.

[62] R. Gütig, H. Sompolinsky, The tempotron: A neuron that learns spike timing-based decisions, *Nature neuroscience* 9 (3)

(2006) 420–428.

- [63] Y. Xu, X. Zeng, S. Zhong, A new supervised learning algorithm for spiking neurons, *Neural computation* 25 (6) (2013) 1472–1511.
- [64] A. Mohemmed, S. Schliebs, S. Matsuda, N. Kasabov, Training spiking neural networks to associate spatio-temporal input–output spike patterns, *Neurocomputing* 107 (2013) 3–10.
- [65] J. Wu, Y. Chua, M. Zhang, Q. Yang, G. Li, H. Li, Deep spiking neural network with spike count based learning rule, in: 2019 International Joint Conference on Neural Networks (IJCNN), IEEE, 2019, pp. 1–6.
- [66] D. Zhao, Y. Zeng, T. Zhang, M. Shi, F. Zhao, Glsnn: A multi-layer spiking neural network based on global feedback alignment and local stdp plasticity, *Frontiers in Computational Neuroscience* 14.